Optics Letters

Silicon arrayed waveguide gratings at 2.0-μm wavelength characterized with an on-chip resonator

Eric J. Stanton,* Nicolas Volet, and John E. Bowers

Department of Electrical and Computer Engineering, University of California, Santa Barbara (UCSB), California 93106, USA
**Corresponding author: estanton@ece.ucsb.edu*

Received 1 December 2017; revised 9 January 2018; accepted 30 January 2018; posted 2 February 2018 (Doc. ID 314760); published 28 February 2018

Low-loss arrayed waveguide gratings (AWGs) are demonstrated at a 2.0-μm wavelength. These devices promote rapidly developing photonic applications, supported by the recent development of mid-infrared lasers integrated on silicon (Si). Multi-spectral photonic integrated circuits at 2.0-μm are envisioned since the AWGs are fabricated with the 500-nm-thick Si-on-insulator platform compatible with recently demonstrated lasers and semiconductor optical amplifiers on Si. Characterization with the AWG-ring method improves the on-chip transmission uncertainty to ∼6% compared to the conventional method with an uncertainty of ∼53%. Channel losses of ∼2.4 dB are found, with −31 dB crosstalk per channel. Fully integrated multi-spectral sources at 2.0 μm with pump lasers, low-loss multiplexers, and an output amplifier are now feasible.

OCIS codes: (060.4230) Multiplexing; (130.7408) Wavelength filtering devices; (140.3298) Laser beam combining.

https://doi.org/10.1364/OL.43.001135

Integrated multi-spectral lasers are an important topic of interest for wavelengths spanning the near- to mid-infrared [1,2]. Such devices have applications near a 2-μm wavelength for communication systems with hollow-core photonic-bandgap fibers (HC-PBFs) [3,4], gas detection and quantification [5], remote sensing [6,7], and infrared countermeasures (IRCM). Water absorption near 2-μm also makes this wavelength important for medical applications [8], such as non-invasive blood glucose measurements [9] and laser surgery [10].

In this scope, an ideal optical source consists of a compact single chip with no free-space optics, which emits high optical power into a near-diffraction-limited beam and covers many spectral bands of interest. Because they are compact, efficient, reliable, and relatively inexpensive, semiconductor lasers are used in nearly every application for which they meet system requirements. Yet, until recently, they were too immature for transitioning to advanced applications such as IRCM, except in limited spectral ranges restricted to the short-wave infrared [11] and the near-visible [12]. This has rapidly changed over the past decade, however, with the advent of aluminum gallium nitride lasers emitting in the ultra-violet [13], interband cascade lasers in the mid-wave infrared [14,15], and quantum cascade lasers in the mid- and long-wave infrared [16]. Nonetheless, even an all-semiconductor source may become complex and cumbersome if free space optics are required to combine multiple beams from several spectral bands. However, on-chip multiplexers with low loss can combine an array of integrated lasers spanning many spectral bands into a single output waveguide to circumvent free-space optics [17].

Arrayed waveguide gratings (AWGs) have proven to have the lowest loss and crosstalk for dense channel spacing (<400 GHz) integrated optical multiplexers. An optical communication system near a 2.0-μm wavelength has been demonstrated with AWGs, based on indium phosphide (InP) waveguides, utilizing the minimum loss window of hollow-core photonic bandgap fibers [4,18]. Communication systems on the Si-on-insulator (SOI) platform could reduce cost and improve performance [19]. Si is an ideal material for high-power 2-μm photonic integrated circuits (PICs) thanks to the low two-photon absorption and high Kerr coefficient [20,21]. Low-loss Si AWGs have been reported in the near- and mid-infrared at different wavelengths (1.6 μm [22], 2.3 μm [23], 3.3 μm [24], and 3.8 μm [25]). Emerging applications require lower-loss AWGs. Improved characterization is also a requisite for evaluating on-chip loss lower than the typical chip-coupling uncertainties (∼2 dB).

This work demonstrates low on-chip loss and crosstalk of an AWG near a 2.0-μm wavelength with 500-nm-thick Si waveguides, compatible with the CW 2.0-μm laser [26] and SOA [27] on Si. Additional analysis is performed to drastically reduce the measurement uncertainty by using an AWG-ring [22] to transmission normalization. The low-loss AWG presented in this work complements the recent demonstrations of a 2.0-μm laser [26], a 2.0-μm SOA [27], and a 2.3-μm photo-diode [28] to further advance PIC capabilities at 2 μm.

The devices are fabricated on a SOI platform [29]. As shown in Fig. 1(a), a 0.50-μm-thick Si layer is used with a 1.00-μm-thick SiO_2 bottom cladding. Features are defined

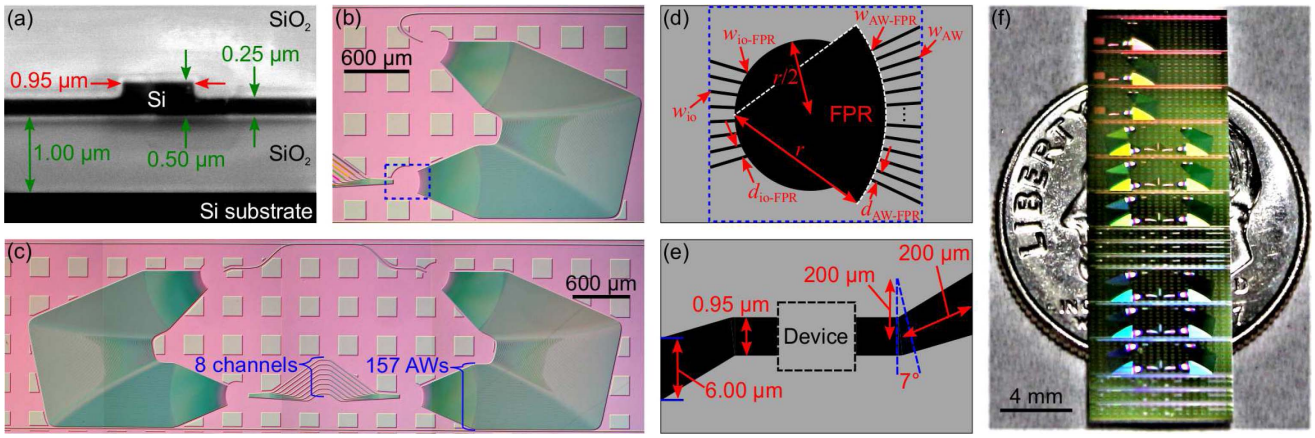

Fig. 1. (a) Cross-section SEM of a single-mode Si waveguide. Micrographs (b) of an AWG and (c) of an AWG-ring. The FPR region outlined with blue in (b) is schematized in (d). (e) Top-view schematic of the facet coupling design. (f) Photograph of the chip on top of a U.S. dime for scale.

with deep-ultraviolet lithography and reactive ion etching with sulfur hexafluoride, oxygen, and argon to remove 0.25 μm of Si. A 4:1 mixture of sulfuric acid and hydrogen peroxide held at 80°C strips the photoresist. A 1.00-μm-thick SiO_2 layer is then sputtered to form the top cladding before dicing the wafer and polishing the facets. Micrographs of the AWG and AWG-ring are shown in Figs. 1(b) and 1(c), respectively. The free propagation region (FPR) with the de-multiplexed and arrayed waveguides is schematized in Fig. 1(d), defining the design parameters listed in Table 1. Other parameters include the number of channels (8) and arrayed waveguides (157). A flared and angled facet waveguide schematized in Fig. 1(e) helps to reduce the fundamental mode reflection. This suppresses the Fabry–Perot resonance amplitude so it does not affect the AWG and AWG-ring transmission spectra. Three copies of each device are photographed on a single chip in Fig. 1(f).

The layout is generated with a unique design process that emphasizes low peak-channel loss over other design parameters, such as the center wavelength of each channel or the footprint size (~3.6 mm^2 for this design) [30]. This contrasts with AWGs typically designed for communication systems, since the current design begins with a different set of assumed parameters [31]. The number of channels, the channel non-uniformity, the center wavelength, and the approximate channel wavelength spacing are decided for the application. All other parameters are derived from these first assumptions; then, the device layout is drawn. Multiple design iterations are performed based on the physical layout dimensions to optimize for low insertion loss. The number of arrayed waveguides is calculated from the angle that encompasses 99% of the power from the input/output (IO) channel waveguide propagation into the FPR. Widths of the arrayed waveguides and IO waveguides at the FPR interface (w_{AW-FPR} and w_{io-FPR}) are chosen to support only one symmetric TE mode. For optimizing the insertion loss, it is important to minimize the excitation from the grating, aside from the designed interference order. For these SOI waveguides, w_{AW-FPR} can be further reduced to decrease the pitch of the arrayed waveguides at the expense of increasing the footprint and, subsequently, the total phase and amplitude noise in the array. However, since the separation of the AWs is set to and limited by the minimum feature size of the lithography process: 0.3 μm, the pitch between i/o waveguides (d_{io-FPR}) is initially estimated to be $2w_{io-FPR}$. Reducing d_{io-FPR} during iteration has two effects: increasing the adjacent channel crosstalk and decreasing the number of arrayed waveguides, which consequently reduces the accumulated phase and amplitude errors. These effects are then balanced to achieve a minimum loss. The channel uniformity is another parameter that can be modified, since this value also affects the number of waveguides and a similar optimization process can be implemented to further reduce the total on-chip loss. Larger values of uniformity reduce the crosstalk and the center channel loss at the expense of the outer channel losses.

Table 1. Design Dimensions for the 2.0-μm AWGs (in μm)

Rowland radius	r	242
AW length increment	ΔL	19.6
AW pitch at FPR	d_{AW-FPR}	1.25
i/o wg. pitch at FPR	d_{io-FPR}	4.20
AW width	w_{AW}	1.20
AW width at FPR	w_{AW-FPR}	1.00
i/o wg. width	w_{io}	0.80
i/o wg. width at FPR	w_{io-FPR}	1.40

The experimental setup is shown in Fig. 2. Light from a diode tunable laser (TL, Newport Velocity TLB-6736) in the wavelength range of 2.004–2.022 μm (driven by a Keithley 2400 SourceMeter) is coupled to a single-mode fiber with an aspheric lens. A polarization controller (PC, Thorlabs PLC-900) is used to excite a transverse-electric (TE) on-chip mode. The light is launched into the integrated waveguide from a lensed fiber (OZ Optics) with an anti-reflective coating centered at a 2.0-μm wavelength. A temperature controller (Newport LDT-5948) holds the chip at 25°C. The transmitted light is collected with another lensed fiber and measured with an optical spectrum analyzer (OSA, Yokogawa AQ6375).

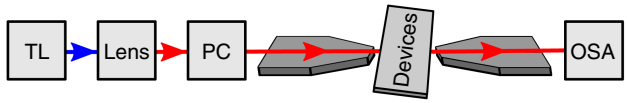

Fig. 2. Schematic of the experimental setup used to measure the transmission spectra of the devices. The red lines indicate single-mode fibers and the blue one represents a free-space collimated beam.

The transmission spectra of 13 straight waveguides are measured to investigate the off- to on-chip coupling efficiency and variation. One example transmission spectrum of these waveguides is presented in Fig. 3(a) in blue and the mean transmission spectrum is shown in black, from which a coupling loss of ~4.5 dB per facet is extracted. The coefficient of variation (V_w), in Fig. 3(b), represents the normalized standard deviation of the straight waveguide transmission. Another measurement of back-scattered light along waveguide spirals near a 1.6-μm wavelength indicates that this variation is dominated by the uncertainty of the facet coupling efficiency [22]. Hence, V_w indicates the normalized uncertainty introduced by the facet coupling, which is used to extract the uncertainty of the on-chip insertion loss from the conventional and AWG-ring methods.

Transmission spectra from two ports of a chip-based unbalanced Mach–Zehnder interferometer (UMZI) are analyzed to characterize the coupler design used in the AWG-ring devices [32]. The extracted transmission coefficient, τ^2, in Fig. 4, is defined as the normalized power transmission.

On-chip AWG transmission spectra, in Fig. 5, are normalized at the peak of each channel to the on-chip transmission values calculated from three separate AWG-rings. An example AWG-ring transmission is shown in Fig. 6, which is used along with the τ^2 values of the coupler to calculate the peak transmission of each AWG channel.

The central channels of the AWG have an on-chip loss of 2.2(3) dB and the uniformity across all eight channels is 0.6(4) dB, where the numbers in parentheses are the standard uncertainties referred to the corresponding last digits of the quoted results. Propagation loss of similar waveguides at 1.6-μm wavelength is ~71 dB/m [22]. The loss at 2.0 μm is expected to be similar or slightly lower since scattering contributes less. Channel crosstalk is calculated across the 3-dB bandwidth of each channel, as detailed in [22], and the average crosstalk per channel is −31 dB. Using a conventional method, the adjacent-channel crosstalk approaches −21 dB. However, the cumulative method is more rigorous and its value represents the crosstalk across channel bandwidth, not just a single wavelength. The

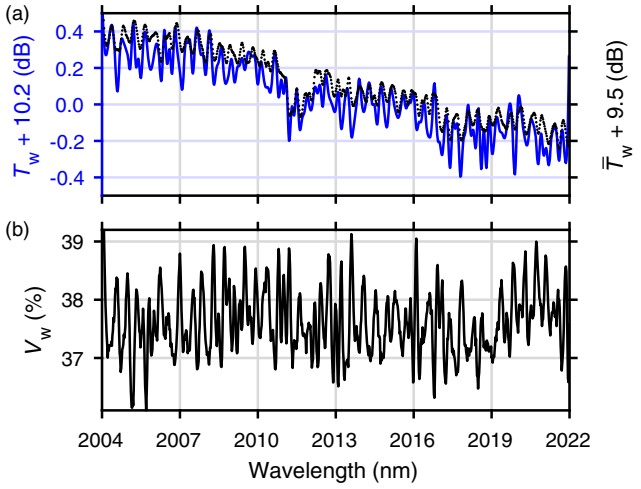

Fig. 3. (a) Transmission spectrum (in black) averaged over 13 straight waveguides and example (in blue). (b) Spectrum of the coefficient of variation V_w, calculated from all straight waveguide transmission spectra.

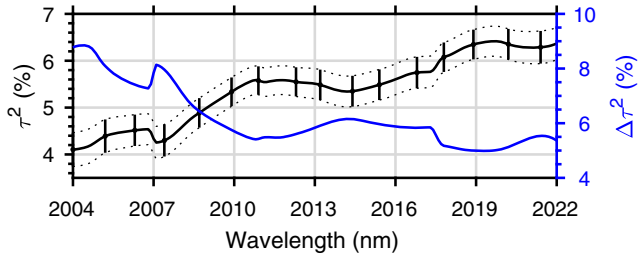

Fig. 4. Spectrum of the transmission coefficient τ^2 for coupling to the AWG-ring, extracted from the spectra of a UMZI, is plotted in black. The uncertainty on this parameter is plotted in blue.

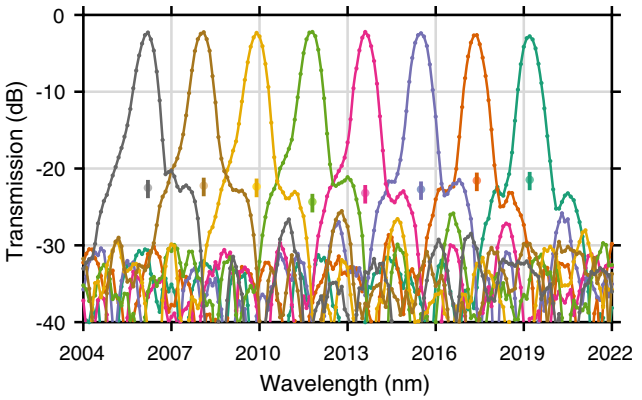

Fig. 5. On-chip transmission spectra measured for the AWG channels, normalized using the AWG-ring method. The 3-dB cumulative crosstalk for each channel is indicated with a dot and the corresponding standard uncertainty is plotted with a vertical line.

conventional normalization method (not shown) is found to have a relative uncertainty of $\langle V_w \rangle \sqrt{2} \approx 53.2\%$ and the AWG-ring method reduces this value to ~6.0%. This uncertainty depends on $\Delta\tau^2$ and on spectral deviations of V_w, which modify the relative minima and maxima in the AWG-ring transmission spectrum, but not on the magnitude of V_w. A detailed formulation is presented in [22]. Note, since the AWG-ring requires two cascaded AWGs, the channel misalignment adds to this uncertainty. By fitting Gaussian curves within the 2-dB bandwidth of the single AWG and the AWG-ring extracted transmissions, the misalignment is calculated as half of the difference in channel widths. A 10(18) pm misalignment is found corresponding to 0.1% of the total transmission uncertainty of 6.0%.

Loss and crosstalk are state-of-the-art for 2.0-μm AWGs [18]. These demonstrations are compatible with heterogeneously integrated lasers on the SOI waveguide platform. The loss of the AWG is due to a combination of waveguide propagation loss and phase error. Absorption in the Si and SiO_2 is negligible compared to the loss from interfacial scattering [20,30]. Therefore, to reduce the total loss of the AWGs and improve the crosstalk, the waveguide sidewall roughness must be reduced. Future work will integrate these AWGs with lasers and a semiconductor optical amplifier, which is estimated to produce >300 mW output power in the fundamental mode [26,27]. This could be increased with more AWG channels or by improving the output

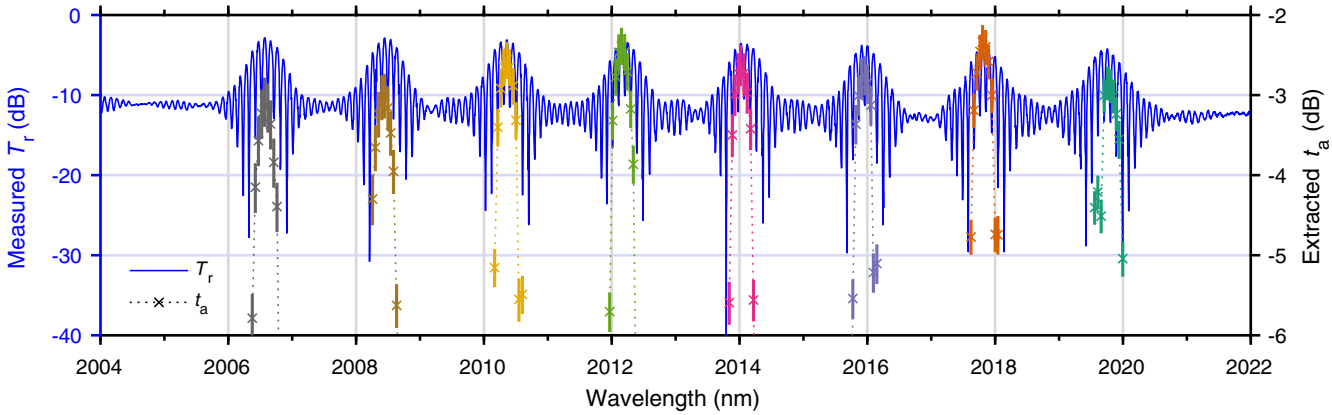

Fig. 6. Measured transmission T_r of an AWG-ring and the extracted transmission t_a of each AWG channel.

power of each laser to make IRCM applications possible. Combining these devices with modulators and detectors would also produce functional systems for gas absorption spectroscopy, optical communications, and medical applications.

Funding. Air Force Research Laboratory (AFRL) (FA8650-17-C-5402).

Acknowledgment. The authors thank the Nanotech staff at UCSB for fabrication support and C. Goldberg at Newport Corporation for support with the tunable laser. N. V. acknowledges support from the Swiss National Science Foundation.

REFERENCES

1. G. Kurczveil, M. J. R. Heck, J. D. Peters, J. M. Garcia, D. Spencer, and J. E. Bowers, IEEE J. Sel. Top. Quantum Electron. **17**, 1521 (2011).
2. C. Gilles, L. J. Orbe, G. Carpintero, G. Maisons, and M. Carras, Opt. Express **23**, 20288 (2015).
3. P. J. Roberts, F. Couny, H. Sabert, B. J. Mangan, D. P. Williams, L. Farr, M. W. Mason, A. Tomlinson, T. A. Birks, J. C. Knight, and P. St.J. Russell, Opt. Express **13**, 236 (2005).
4. Y. Chen, Z. Liu, S. R. Sandoghchi, G. T. Jasion, T. D. Bradley, E. N. Fokoua, J. R. Hayes, N. V. Wheeler, D. R. Gray, B. J. Mangan, R. Slavìk, F. Poletti, M. N. Petrovich, and D. J. Richardson, J. Lightwave Technol. **34**, 104 (2016).
5. A. Khan, D. Schaefer, L. Tao, D. J. Miller, K. Sun, M. A. Zondlo, W. A. Harrison, B. Roscoe, and D. J. Lary, Remote Sens. **4**, 1355 (2012).
6. R. J. De Young and N. P. Barnes, Appl. Opt. **49**, 562 (2010).
7. S. Ishii, K. Mizutani, H. Fukuoka, T. Ishikawa, B. Philippe, H. Iwai, T. Aoki, T. Itabe, A. Sato, and K. Asai, Appl. Opt. **49**, 1809 (2010).
8. K. Scholle, S. Lamrini, P. Koopmann, and P. Fuhrberg, in *Frontiers in Guided Wave Optics and Optoelectronics*, B. Pal, ed. (InTech, 2010), Chap. 21, pp. 471–500.
9. N. V. Alexeeva and M. A. Arnold, J. Diabetes Sci. Technol. **3**, 219 (2009).
10. B. Chen, S. L. Thomsen, R. J. Thomas, J. Oliver, and A. J. Welch, Lasers Surg. Med. **40**, 358 (2008).
11. H. K. Choi and S. J. Eglash, Appl. Phys. Lett. **61**, 1154 (1992).
12. M. Sakamoto, J. G. Endriz, and D. R. Scifres, Electron. Lett. **28**, 197 (1992).
13. H. Yoshida, Y. Yamashita, M. Kuwabara, and H. Kan, Nat. Photonics **2**, 551 (2008).
14. M. Kim, C. L. Canedy, W. W. Bewley, C. S. Kim, J. R. Lindle, J. Abell, I. Vurgaftman, and J. R. Meyer, Appl. Phys. Lett. **92**, 191110 (2008).
15. W. W. Bewley, C. L. Canedy, C. S. Kim, M. Kim, C. D. Merritt, J. Abell, I. Vurgaftman, and J. R. Meyer, Opt. Express **20**, 20894 (2012).
16. Y. Yao, A. J. Hoffman, and C. F. Gmachl, Nat. Photonics **6**, 432 (2012).
17. E. J. Stanton, M. J. R. Heck, J. Bovington, A. Spott, and J. E. Bowers, Opt. Express **23**, 11272 (2015).
18. H. Zhang, M. Gleeson, N. Ye, N. Pavarelli, X. Ouyang, J. Zhao, N. Kavanagh, C. Robert, H. Yang, P. Morrissey, K. Thomas, A. Gocalinska, Y. Chen, T. Bradley, J. Wooler, J. Hayes, E. Numkam Fokoua, Z. Li, S. Alam, F. Poletti, M. Petrovich, D. Richardson, B. Kelly, J. O'Carrol, R. Phelan, E. Pelucchi, P. O'Brian, F. Peters, B. Corbett, and F. Gunning, Opt. Lett. **40**, 3308 (2015).
19. G. Roelkens, A. Abassi, P. Cardile, U. Dave, A. De Groote, Y. De Koninck, S. Dhoore, X. Fu, A. Gassenq, N. Hattasan, Q. Huang, S. Kumari, S. Keyvaninia, B. Kuyken, L. Li, P. Mechet, M. Muneeb, D. Sanchez, H. Shao, T. Spuesens, A. Z. Subramanian, S. Uvin, M. Tassaert, K. van Gasse, J. Verbist, R. Wang, Z. Wang, J. Zhang, J. van Campenhout, X. Yin, J. Bauwelinck, G. Morthier, R. Baets, and D. Van Thourhout, Photonics **2**, 969 (2015).
20. R. A. Soref, S. J. Emelett, and W. R. Buchwald, J. Opt. A **8**, 840 (2006).
21. A. D. Bristow, N. Rotenberg, and H. M. Van Driel, Appl. Phys. Lett. **90**, 191104 (2007).
22. E. J. Stanton, N. Volet, and J. E. Bowers, Opt. Express **25**, 30651 (2017).
23. R. Wang, M. Muneeb, S. Sprengel, G. Boehm, A. Malik, R. Baets, M.-C. Amann, and G. Roelkens, Opt. Express **24**, 8480 (2016).
24. R. Wang, A. Vasiliev, M. Muneeb, A. Malik, S. Sprengel, G. Boehm, M.-C. Amann, I. Šimonytė, A. Vizbaras, K. Vizbaras, R. Baets, and G. Roelkens, Sensors **17**, 1788 (2017).
25. M. Muneeb, X. Chen, P. Verheyen, G. Lepage, S. Pathak, E. Ryckeboer, A. Malik, B. Kuyken, M. Nedeljkovic, J. Van Campenhout, G. Z. Mashanovich, and G. Roelkens, Opt. Express **21**, 11659 (2013).
26. A. Spott, M. Davenport, J. Peters, J. Bovington, M. J. R. Heck, E. J. Stanton, I. Vurgaftman, J. Meyer, and J. Bowers, Opt. Lett. **40**, 1480 (2015).
27. N. Volet, A. Spott, E. J. Stanton, M. L. Davenport, L. Chang, J. D. Peters, T. C. Briles, I. Vurgaftman, J. R. Meyer, and J. E. Bowers, Laser Photon. Rev. **11**, 1600165 (2017).
28. R. Wang, S. Sprengel, M. Muneeb, G. Boehm, R. Baets, M.-C. Amann, and G. Roelkens, Opt. Express **23**, 26834 (2015).
29. K. Okamoto, IEEE J. Sel. Top. Quantum Electron. **20**, 248 (2014).
30. E. Stanton, A. Spott, M. Davenport, N. Volet, and J. Bowers, Opt. Lett. **41**, 1785 (2016).
31. S. Pathak, D. Van Thourhout, and W. Bogaerts, Opt. Lett. **38**, 2961 (2013).
32. M. A. Tran, T. Komljenovic, J. C. Hulme, M. L. Davenport, and J. E. Bowers, IEEE Photon. Technol. Lett. **28**, 1517 (2016).